JBC RESEARCH ARTICLE

Structural characterization of HIV-1 matrix mutants implicated in envelope incorporation

Received for publication, October 13, 2020, and in revised form, January 5, 2021 Published, Papers in Press, January 22, 2021,
https://doi.org/10.1016/j.jbc.2021.100321

Gunnar N. Eastep, Ruba H. Ghanam, Todd J. Green, and Jamil S. Saad*
From the Department of Microbiology, University of Alabama at Birmingham, Birmingham, Alabama, USA

Edited by Karin Musier-Forsyth

During the late phase of HIV-1 infection, viral Gag polyproteins are targeted to the plasma membrane (PM) for assembly. Gag localization at the PM is a prerequisite for the incorporation of the envelope protein (Env) into budding particles. Gag assembly and Env incorporation are mediated by the N-terminal myristoylated matrix (MA) domain of Gag. Nonconservative mutations in the trimer interface of MA (A45E, T70R, and L75G) were found to impair Env incorporation and infectivity, leading to the hypothesis that MA trimerization is an obligatory step for Env incorporation. Conversely, Env incorporation can be rescued by a compensatory mutation in the MA trimer interface (Q63R). The impact of these MA mutations on the structure and trimerization properties of MA is not known. In this study, we employed NMR spectroscopy, X-ray crystallography, and sedimentation techniques to characterize the structure and trimerization properties of HIV-1 MA A45E, Q63R, T70R, and L75G mutant proteins. NMR data revealed that these point mutations did not alter the overall structure and folding of MA but caused minor structural perturbations in the trimer interface. Analytical ultracentrifugation data indicated that mutations had a minimal effect on the MA monomer–trimer equilibrium. The high-resolution X-ray structure of the unmyristoylated MA Q63R protein revealed hydrogen bonding between the side chains of adjacent Arg-63 and Ser-67 on neighboring MA molecules, providing the first structural evidence for an additional intermolecular interaction in the trimer interface. These findings advance our knowledge of the interplay of MA trimerization and Env incorporation into HIV-1 particles.

During the late phase of HIV-1 replication, the viral Gag polyproteins are targeted to the plasma membrane (PM) for particle budding and release (1–7). Binding of HIV-1 Gag polyproteins to the inner leaflet of the PM is mediated by the matrix (MA) domain, which harbors a bipartite signal represented by an N-terminal myristoyl (myr) group and a highly basic region (HBR). It is demonstrated that HIV-1 Gag association with membranes is regulated by multiple factors including electrostatic and hydrophobic interactions, protein multimerization, cellular and viral RNA, and specific phospholipids such as phosphatidylinositol 4,5-bisphosphate (PI(4,5)P_2) (7–13). Gag binding to membranes is also enhanced by inclusion of phosphatidylserine (PS) and cholesterol (6, 8, 9, 12, 14–20).

Pioneering X-ray crystallography studies of HIV-1 unmyristoylated MA [myr(−)MA] revealed that the protein adopts a trimer arrangement (21). However, solution NMR studies indicated that myr(−)MA is monomeric at all tested protein concentrations (22–27). On the other hand, sedimentation equilibrium data confirmed that the MA protein resides in monomer–trimer equilibrium. NMR–based structural studies have shown that the myr group of MA can adopt sequestered and exposed conformations (26). Extrusion of the myr group can be increased by factors that promote protein self-association, such as increasing protein concentration or inclusion of the capsid (CA) domain (26). Subsequent studies revealed that myr exposure in MA is promoted by binding of PI(4,5)P_2 (25) and is regulated by pH (27). In an attempt to characterize the trimeric form of MA, we recently engineered a stable recombinant protein construct by fusing a foldon domain (FD) of phage T4 fibritin to the MA C terminus (28). The FD domain is a 30-amino acid segment that forms a β-sheet propeller consisting of monomeric β-hairpin segments (29, 30). Hydrogen–deuterium exchange mass spectrometry (HDX-MS) data supported an MA–MA interface that is consistent with that observed in the crystal structure of the myr(−)MA trimer (28). A plethora of structural and biophysical studies have provided invaluable insights into retroviral MA proteins binding to phospholipids and membrane mimetics (23–25, 31–40). These studies identified key molecular determinants of MA–membrane interactions and advanced our knowledge of retroviral assembly.

Studies by Barklis and coworkers revealed that the HIV-1 MA and MACA proteins assemble as hexagonal cage lattices on PS/cholesterol membrane monolayers and as hexamers of trimers in the presence of PI(4,5)P_2 (41–43). The hexamer of trimers assembly is increasingly used as a model to explain the mechanism by which the envelope (Env) protein is incorporated into virus particles (44–47). In its processed form, Env consists of two noncovalently associated subunits, a surface glycoprotein (gp120) and a transmembrane domain (gp41), which are products of proteolytic cleavage of the viral gp160 precursor protein (reviewed in [48–50]). There is strong evidence that the cytoplasmic tail of gp41 (gp41CT) plays a

This article contains supporting information.
* For correspondence: Jamil S. Saad, saad@uab.edu.

functional role in Env incorporation in physiologically relevant cell types (44, 46, 47, 51–54). NMR studies of the HIV-1 gp41CT protein revealed that the N-terminal 45 residues lack secondary structure and are not associated with the membrane. The C-terminal 105 residues, however, form three membrane-bound amphipathic α-helices with distinctive structural features such as variable degree of membrane penetration, hydrophobic and basic surfaces, clusters of aromatic residues, and a network of cation–π interactions (55). Recent NMR studies suggested dynamic coupling across the transmembrane, between the ectodomain and CT (56).

Genetic and biochemical studies suggested that the MA domain of Gag and the gp41CT play distinct, yet complementary, roles in Env incorporation into budding particles (44, 46, 47, 51, 52, 57–62). Point mutations in MA (L13E, E17K, L31E, V35E, or E99V) were found to impair Env incorporation in HIV-1 particles (44–46, 52, 59). [Note: The N-terminal Met, which is absent in the myristoylated protein, is designated as residue 1. In contrast, other studies considered the N-terminal Gly of the myristoylated protein as residue 1]. When mapped on the putative hexamer of trimer model of MA, these residues were found to point toward the hexamer centers (Fig. 1) (41, 42). It was also shown that substitution of residue Gln^{63} with Arg suppressed Env incorporation defects of the L13E, E17K, L31E, V35E, or E99V MA mutations and of a gp41CT mutation that has the same phenotype (44–46, 52). Freed and coworkers provided biochemical evidence that MA trimerization is an obligatory step in the assembly of infectious HIV-1 and demonstrated a correlation between loss of MA trimerization and loss of Env incorporation (46). It was suggested that the Q63R mutation may stabilize the trimer structure such that MA lattices, which form large hexamer holes, are favored over those that feature small hexamer holes (Fig. 1) (46). In another study, biochemical and pull-down experiments suggested that the Q63R mutation promoted interaction with gp41CT; this mutation did not alter the organization of MA on a membrane monolayer (43). Nonconservative mutations at positions Ala^{45}, Ser^{72}, and Leu^{75} located in the trimer interface (Fig. 1) also impaired Env incorporation and infectivity, and biochemical cross-linking experiments showed that these mutations reduced trimerization of MA (46). Although genetic and biochemical studies provided evidence for a correlation between Env incorporation and formation of MA trimers, the structural or biophysical evidence for such a correlation is lacking. In particular, it is not known how single amino acid mutations that impair or rescue Env incorporation impact the structure and oligomerization properties of MA.

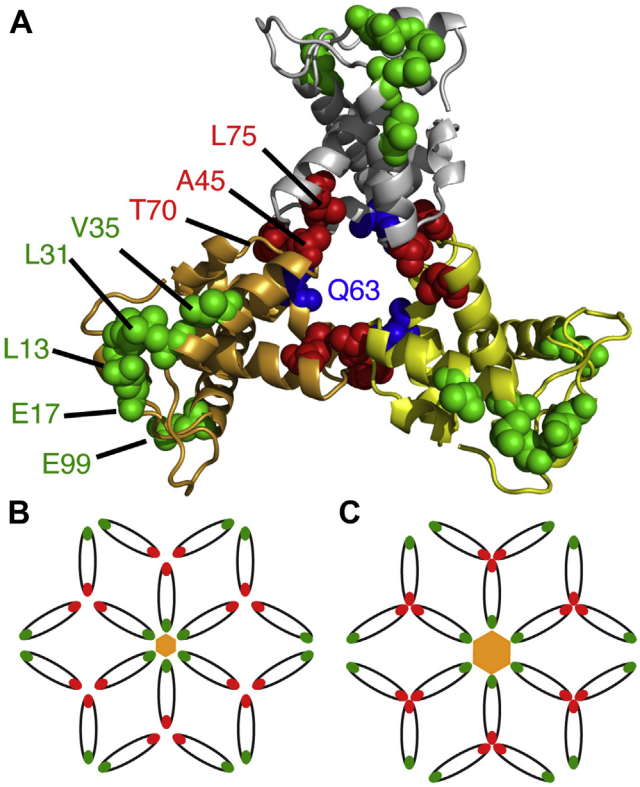

Figure 1. MA trimer model and residues implicated in Env incorporation. *A*, structure of the myr(–)MA trimer (PDB ID: 1HIW) showing residues implicated in Env incorporation (*green*, *blue*, and *red spheres*). *B*, schematic representation of the hexamer of trimer arrangement of MA based on studies by Alfadhli *et al.* (41) and adopted by Freed *et al.* (46). In this model, a ∼45 nm central aperture is formed by residues at the center of the hexamer (*green*). It is suggested that the gp41CT protein is accommodated in the central aperture. Mutations of residues in the trimer interface (*red spheres*) significantly disrupted Env incorporation. *C*, perturbations of the putative hexamer or trimer interface in the MA lattice are thought to create smaller central aperture (∼30 nm) that may cause a steric exclusion of gp41CT.

In this report, we employed NMR spectroscopy, X-ray crystallography, and analytical ultracentrifugation (AUC) techniques to characterize the structure and trimerization properties of HIV-1 MA mutants that have been shown to impair Env incorporation (L75G, A45E, and T70R) or suppress Env incorporation defects (Q63R). We show that these mutations had no adverse effect on the structure or folding of MA and had only a minimal effect on the monomer–trimer equilibrium. NMR data revealed that these amino acid substitutions caused chemical shift perturbations (CSPs) for residues located in the trimer interface. The X-ray structure of myr(–)MA Q63R protein revealed hydrogen bonding between the side chains of adjacent Arg^{63} and Ser^{67} on neihbouring MA molecules located in the trimer interface. These findings advance our knowledge of the interplay of MA trimerization and Env incorporation into HIV-1 particles.

Results

Effect of point mutations on the structure of MA

Point mutations in the HIV-1 MA protein (A45E, Q63R, T70R, and L75G) were made by site-directed mutagenesis of the MA gene embedded in a coexpression vector harboring yeast N-myristoyltransferase (26). Point mutations had no detectable effect on protein expression or the efficiency of myristoylation, which was judged by the elution profile of the protein from the hydrophobic interaction column. Two-dimensional (2D) ^{1}H-^{15}N HSQC NMR spectrum provides a structure-sensitive signal for each amide group in a protein, and thus, it can be used to report on changes to protein structure caused by amino acid substitutions. As shown in Figures 2 and S1, the HSQC spectra for the four MA mutant

proteins are very similar to the spectrum of the wild-type (WT) protein, indicating that amino acid substitutions had no adverse effect on the structure and folding of the protein.

Effect of amino acid substitutions on the myr switch

Previous NMR studies of the WT MA protein have shown that a subset of ^{1}H and ^{15}N resonances for amino acid residues 3–18, Val^{35}, Trp^{36}, Arg^{39}, Gly^{49}, Glu^{52}, His^{89}, and Gln^{90} shift progressively toward the corresponding frequencies observed for myr(−)MA upon increasing protein concentration. These chemical shifts were attributed to exposure of the myr group and a concomitant shift in the monomer–trimer equilibrium toward the trimeric species (26). Subsequent NMR studies revealed that point mutations in the N-terminal region of MA (*e.g.*, V7R, L8A, or L8I) that impaired membrane targeting of Gag and inhibited virus assembly and release (63–66) did not

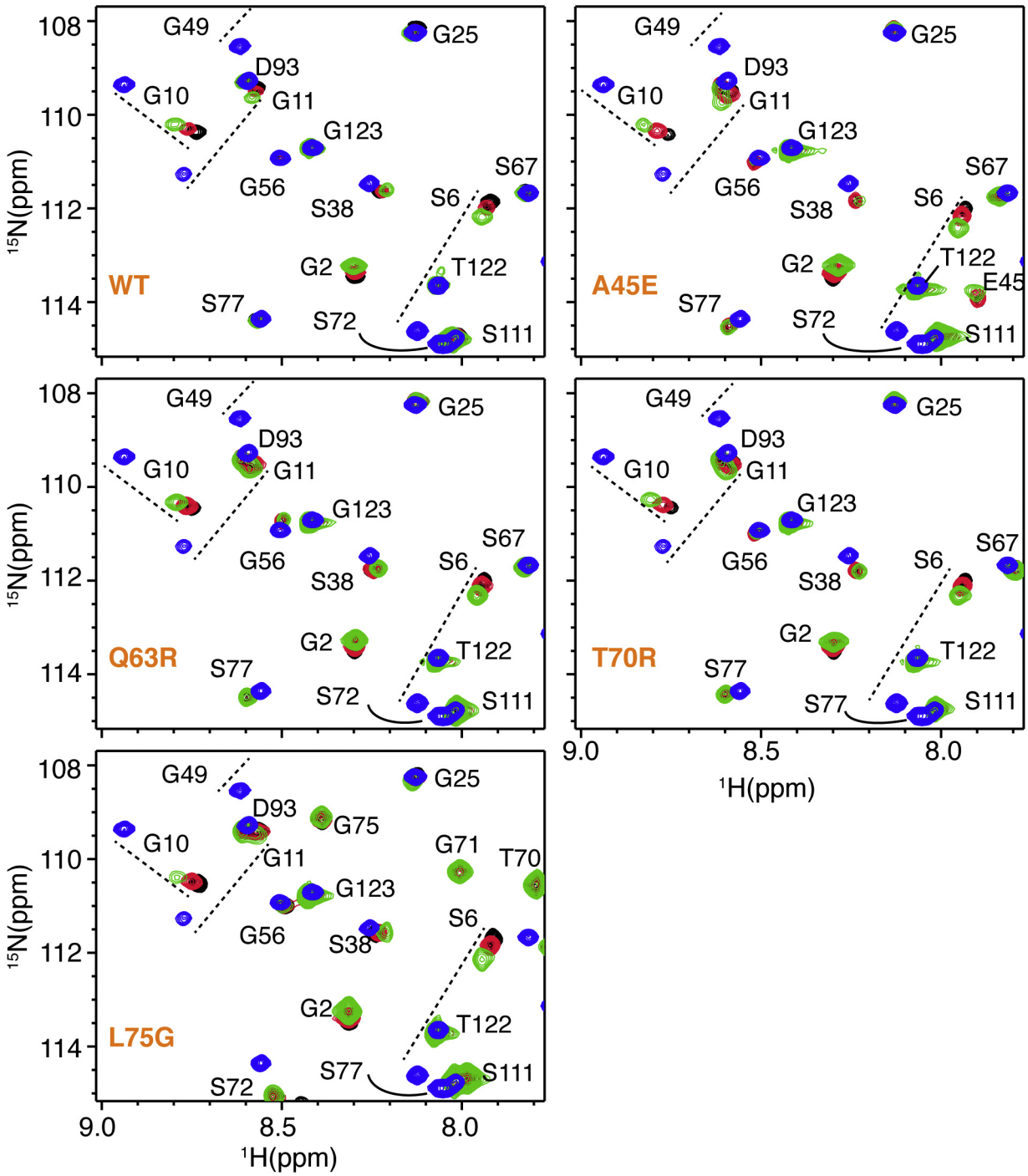

Figure 2. NMR spectra of WT and mutant MA at different protein concentrations. Overlay of 2D ^{1}H-^{15}N HSQC spectra for WT, myr(−), and mutant MA proteins collected at different concentrations (50 μM [*black*], 150 μM [*red*], and 450 μM [*green*]). Like WT MA, for all four mutant proteins a subset of ^{1}H-^{15}N resonances of MA shifted toward the corresponding signals of myr(−)MA (*blue*), indicating a shift in equilibrium toward the myr-exposed state.

exhibit concentration-dependent myristate exposure (24). Structural data revealed conformational changes that appeared to be responsible for stabilizing the myristate-sequestered species and inhibiting exposure (24). Herein, we assessed whether the A45E, Q63R, T70R and L75G mutations in MA had any effect on the positioning of the myr group and/or the concentration-dependent myr-exposure. We obtained ^{1}H-^{15}N HSQC spectra for WT and A45E, Q63R, T70R, and L75G mutant MA proteins at three protein concentrations (50, 150, and 450 μM) (Figs. 2 and S2). Like WT MA, for all mutants the ^{1}H and ^{15}N resonances for residues 3–18, Val^{35}, Trp^{36}, Arg^{39}, Gly^{49}, Glu^{52}, His^{89}, and Gln^{90} were sensitive to protein

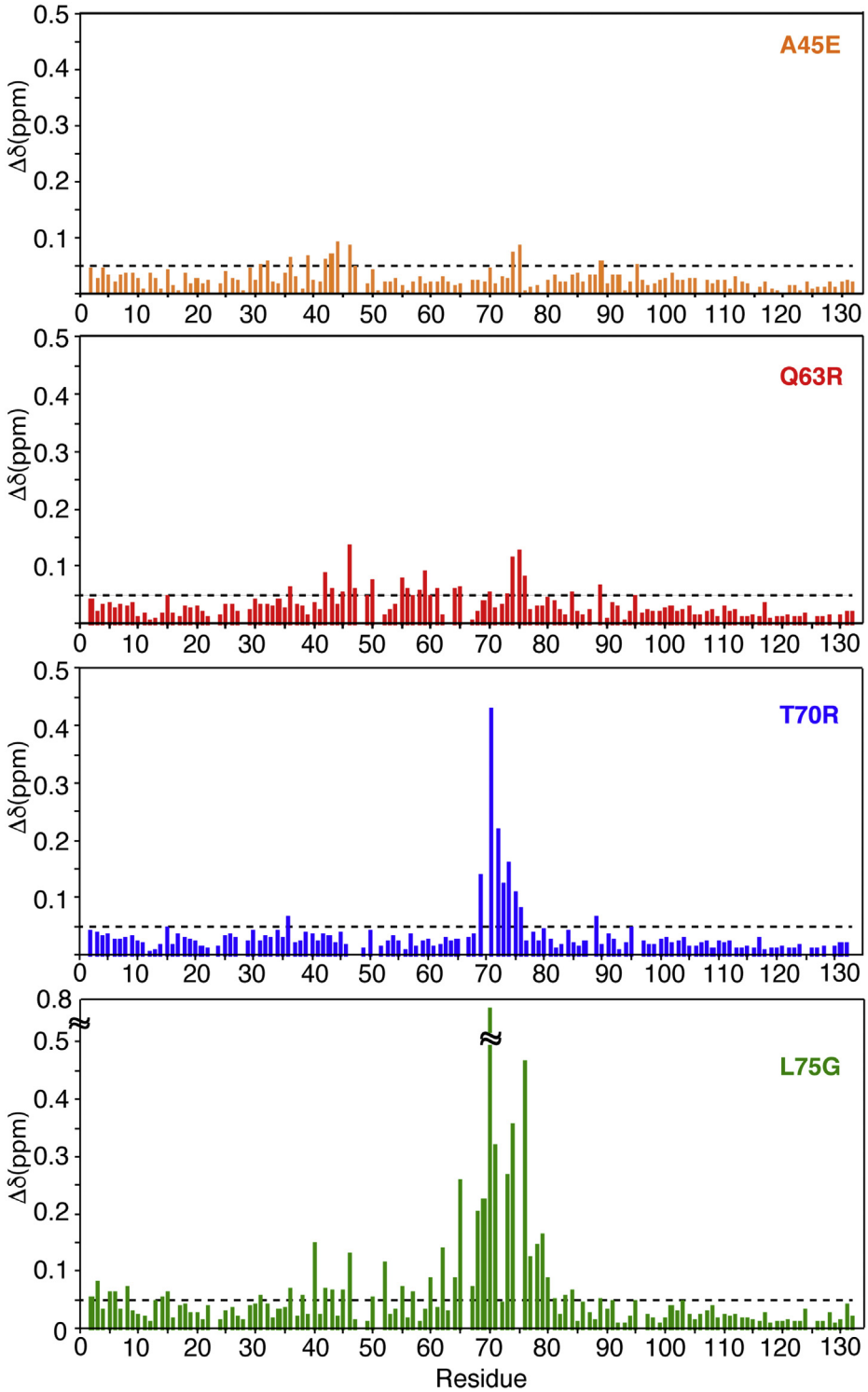

Figure 3. Chemical shift differences between the WT and mutant MA proteins. Normalized ^{1}H-^{15}N chemical shift differences are plotted *versus* residue number. Δδ > 0.05 ppm indicates significant chemical shift changes. NMR spectra were collected at 150 μM.

concentration and shifted progressively toward the corresponding resonances observed for myr(−)MA upon increasing protein concentration (Figs. 2 and S2). Of note, although these signals shift toward the corresponding resonances of the myr(−)MA protein, the chemical shifts for these residues in the fully myr-exposed form of MA may not be at identical positions. Therefore, it is not possible to determine the population of the monomer and trimer states from the NMR data. However, based on the monomer–trimer association constants described below, it is estimated that the trimer population is ∼10%, 35%, and 63% at 50, 150, and 450 μM, respectively. Altogether, these results indicate that none of the four amino acid substitutions had any detectable effect on the concentration-dependent myr switch.

Chemical shift comparison between the WT and mutant MA proteins

To compare the backbone ^{1}H, ^{15}N and ^{13}C chemical shifts with those of the WT MA protein, triple-resonance experiments were collected for all mutants. We mapped the ^{1}H and ^{15}N chemical shift changes caused by amino acid substitutions in MA and assessed whether they induced structural and/or conformational changes in distant regions of the MA protein, especially within the trimer interface. Typically, only a few signals corresponding to amino acids in the vicinity of the mutation site exhibit major chemical shift changes in the ^{1}H-^{15}N HSQC spectrum. Chemical shift differences between the WT and mutant MA proteins are provided in Figure 3, and a cartoon representation of the X-ray structure of the WT MA protein onto which the locations of residues that exhibited significant amide ^{1}H-^{15}N chemical shift change are mapped (Fig. 4). As expected, the largest differences are observed in the vicinity of mutation site. Interestingly, other regions that are distant from the mutation site were also perturbed. For the A45E mutant, in addition to the CSPs observed for signals of residues 39–47, which are in the vicinity of the mutation site, resonances corresponding to Glu^{74} and Leu^{75} also exhibited significant CSPs (Fig. 3). Interestingly, these two residues are quite distant from the mutation site within the same molecule but are intermolecularly adjacent (∼4.5 Å) in the trimer structure of myr(−)MA (Fig. 4). This result suggests that substitution of Ala^{45} to Glu may have induced structural perturbations in the trimer interface. Next, we examined the Q63R mutant. Gln^{63} is located in α-helix IV, with its side chain projecting toward the loop comprised of residues 42–46 (∼4.1 Å to residue Val^{46}) within the same molecule. As shown in Figure 3, in addition to the mutation site, two other regions exhibited significant CSPs. These comprise residues 42–47 and 74–76. Mapping out the CSPs on the trimer structure of myr(−)MA revealed that this mutation can cause structural perturbations for residues 42–46 within the same molecule (Fig. 4). Therefore, it is likely that the CSPs corresponding to residues 42–46 are caused by intramolecular structural adjustments or

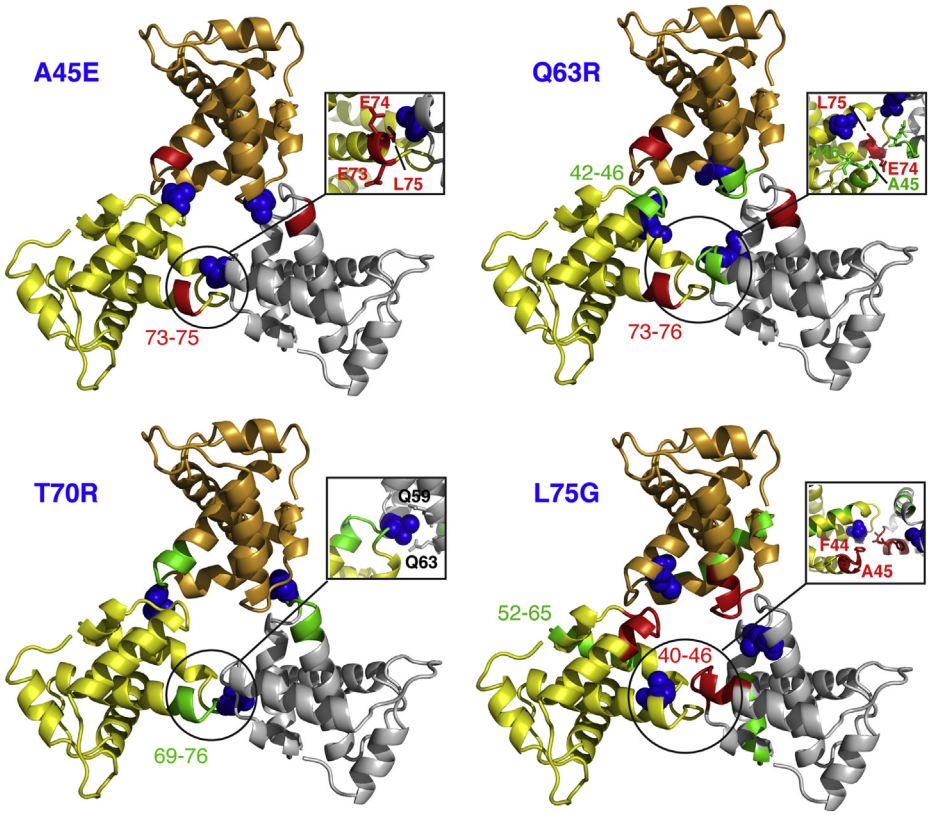

Figure 4. Chemical shift mapping on the structure of the myr(−)MA trimer. Structural mapping of the chemical shift differences onto the X-ray structure of WT MA trimer (PDB ID: 1HIW). The location of the amino acid mutation is marked with *blue spheres*. Positions of residues whose amide resonances exhibited $\Delta\delta > 0.05$ ppm are highlighted in *red* (intermolecular) and *green* (intramolecular).

perturbations as a result of this substitution. However, whereas amino acid residues 74–75 are intramolecularly distant from Gln[63], these residues are located in the trimer interface (Fig. 4). In this case, the effect of Q63R mutation could be direct on residues 74–76 or indirect through a local structural perturbation of residues 42–47, which are also close to residues 74–76 (Fig. 4).

Among the four mutants, the largest CSPs have been observed in the HSQC spectra of the MA T70R and L75G proteins (Fig. 3). For T70R, the most significant CSPs are for residues localized in the vicinity of the mutation site (amino acid residues 69–76). Structural analysis of the MA trimer revealed that the side chain of Thr[70], which resides in the loop connecting α-helices IV and V, is sandwiched between the side chains of Gln[59] and Gln[63] of a neighboring molecule (Fig. 4). Interestingly, the amide ^{1}H-^{15}N resonances of these two residues did not exhibit significant chemical shift changes. On the other hand, mutation of Leu[75] to Gly induced substantial CSPs that extended beyond the mutation site, including residues in the trimer interface (Figs. 3 and 4). Of note, residue Leu[75], located in helix V, is not involved in intermolecular interactions with a neighboring molecule. However, within the same molecule, the side chain of Leu[75] is relatively close to the side chain of Leu[64] located in helix V (4 Å) and is spatially close to the loop made of residues 67–72. As discussed above, residues 67–72 are located in the trimer interface and are in close proximity to the loop made of residues 43–47. Therefore, it is conceivable that Leu[75] contributes to the orientation of the loop.

Taken together, NMR data provided insights into structural perturbations within the trimer interface induced by the amino acid substitutions. However, we were unable to precisely determine these structural changes in the trimer interface by NMR methods because, like the WT MA protein (26), detection of intermolecular contacts (*e.g.*, NOE) proved to be technically challenging. In summary, we provided structural evidence that substitution of amino acid residues in the trimer interface can directly or indirectly contribute to the (de)stabilization of the MA trimer form.

Table 1
X-ray diffraction and refinement statistics

Parameter	Crystal 1	Crystal 2
Wavelength	1.000	1.000
Resolution range	46.21–2.04 (2.113–2.04)	36.82–2.35 (2.434–2.35)
Space group	P 1 21 1	P 1 21 1
Unit cell	63.13 97.92 84.81 90 99.94 90	64.54 90.72 73.16 90 102.38 90
Total reflections	171742	100393
Unique reflections	61,490 (6078)	32,573 (3286)
Multiplicity	2.8	3.1
Completeness (%)	95.03 (94.19)	94.51 (95.36)
Mean I/sigma(I)	28.86 (2.50)	25.95 (2.38)
Wilson B-factor	42.84	49.51
R-merge	0.067 (0.408)	0.072 (0.431)
R-meas	0.083 (0.508)	0.088 (0.515)
R-pim	0.048 (0.298)	0.050 (0.277)
CC1/2	0.987 (0.726)	0.987 (0.807)
Reflections used in refinement	61,481 (6078)	32,566 (3285)
Reflections used for R-free	1995 (197)	1999 (202)
R-work	0.2032 (0.2525)	0.2170 (0.2481)
R-free	0.2340 (0.3166)	0.2560 (0.2723)
Number of non-hydrogen atoms	5507	5286
macromolecules	5141	5111
Ligands	149	108
Solvent	217	67
Protein residues	638	632
RMS(bonds)	0.008	0.008
RMS(angles)	1.2	1.07
Ramachandran favored (%)	100	98.06
Ramachandran allowed (%)	0.00	1.61
Ramachandran outliers (%)	0.00	0.32
Rotamer outliers (%)	1.07	3.22
Clashscore	5.99	8.92
Average B-factor	51.98	65.77
macromolecules	51.67	65.83
Ligands	59.99	65.32
Solvent	53.77	61.45
Number of TLS groups	40	29

The values in parentheses correspond to the highest resolution data shell.

Crystal structure of the myr(–)MA Q63R protein

As discussed above, to explain the role of MA trimerization in Env incorporation, it was suggested that the Q63R mutation in MA may stabilize the trimer structure such that MA lattices that form large hexamer holes are favored over those that feature small hexamer holes (Fig. 1) (46). However, it is not clear how this substitution can stabilize the trimer form. We have shown that, similar to the WT MA protein, MA Q63R is in monomer–trimer equilibrium. As indicated by the NMR data, substitution of Gln[63] to Arg did not induce significant CSPs of residues in the trimeric interface. To be able to assess the structural changes in the MA trimer, we determined the high-resolution structure of myr(–)MA Q63R protein by X-ray crystallography. Atomic coordinates and structure factors for two crystal forms have been deposited in the PDB (codes 7JXR and 7JXS; Table 1). Interestingly, the two crystal forms of myr(–)MA Q63R yielded structures that are essentially identical with slightly different parameters (Fig. S3 and Table 1). Each asymmetric unit of the crystal structure contains two trimers. The structure of the myr(–)MA Q63R trimer in both crystal forms is virtually identical to that of the WT myr(–)MA protein with slight orientation differences of monomers in the trimeric assembly (Fig. 5) (21). The structures in the two crystal forms revealed only minor conformational changes in the loops connecting helices I and II and helices V and VI (Fig. S3). Intriguingly, the guanidinium group of Arg[63] is 2.5 Å (averaged across 12 examples in the asymmetric unit of the two crystal forms) from the hydroxyl group of Ser[67] of an adjacent MA molecule, which forms new hydrogen bonding in the trimer interface (Fig. 5). This result demonstrates that substitution of Gln[63] with Arg stabilizes the trimer structure of MA in the crystal lattice through H-bonding between the side chains of Arg[63] and Ser[67] located on two neighboring MA molecules.

Oligomeric properties of MA mutants

As mentioned earlier, previous sedimentation equilibrium (SE) studies have shown that, while myr(–)MA is monomeric at all tested protein concentrations and pH values (22–27), the

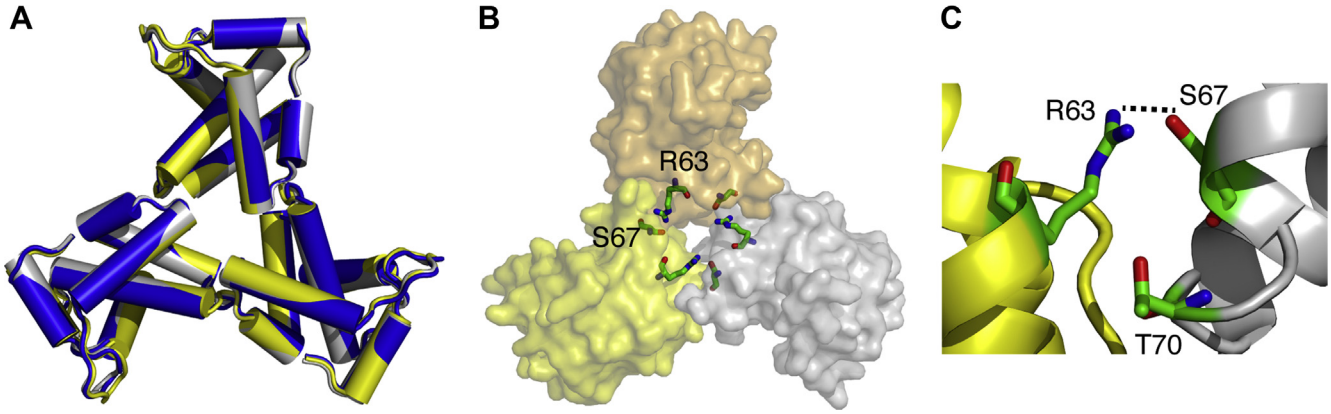

Figure 5. High-resolution crystal structure of the HIV-1 myr(–)MA Q63R protein. *A*, superposition of WT myr(–)MA trimer protein (PDB code 1HIW; *blue*) and the two trimers found in the asymmetric unit of the crystal structure of myr(–)MA Q63R (*yellow* and *gray*). The structure of the myr(–)MA Q63R mutant is essentially identical to that of the WT myr(–)MA protein. *B*, surface representation of the trimer arrangement of the myr(–)MA Q63R protein. Amino acid residues Arg^{63} and Ser^{67} are shown as sticks. *C*, cartoon representation of myr(–)MA Q63R mutant showing the H-bond formed between the side chains of Arg^{63} and Ser^{67}. Residue Thr^{70} is also shown to highlight the close proximity to Arg^{63}.

MA protein is in monomer–trimer equilibrium (24, 26), a process that is modulated by changing solution pH (27). These results were explained by a (de)protonation process of the His^{89} imidazole ring. Deprotonation of His^{89} destabilizes the salt bridge formed between His^{89}(Hδ2) and Glu^{12}(COO-), leading to tight sequestration of the myr group and a shift in the equilibrium from trimer to monomer. To determine how the various MA mutations impacted the oligomerization properties of the MA protein in solution, we collected sedimentation velocity (SV) and SE data on the WT and mutant MA proteins at pH 5.5. Consistent with previous data, the SV profile for myr(–)MA exhibits a sharp sedimentation boundary indicating a monomeric state (Fig. 6). The MA protein, however, exhibits a broad sedimentation boundary with a larger S value consistent with a monomer–trimer equilibrium. The MA mutants exhibited slightly variable sedimentation boundaries with an overall sedimentation coefficient (c(s)) distribution similar to that of the WT MA protein. Interestingly, the sedimentation boundary for the L75G mutant is sharper than the WT and the other mutants and shifted to a smaller S value, suggesting that the monomer–trimer equilibrium is shifted toward the monomeric form (Fig. 6). Next, we collected SE data for the WT and mutant MA proteins at pH 5.5 (Fig. S4). Like the WT protein, SE data for all mutants best fit a monomer–trimer model. Interestingly, while the K_a values for the A45E, T70R, and Q63R mutant proteins are similar to the WT protein, the corresponding value for the L75G mutant is approximately twofold lower (Table 2), consistent with a lower trimer population. Taken together, the SV and SE data indicate that whereas none of the four mutations in MA significantly altered the monomer–trimer equilibrium in solution, the L75G mutation appears to shift the equilibrium toward the monomer form.

Discussion

Point mutations of MA residues Leu^{13}, Glu^{17}, Leu^{31}, Val^{35}, and Glu^{99}, located at the tip of the hexamer centers in the hexamer of trimer model (Fig. 1), were found to impair Env incorporation without affecting virus particle formation (57–60). Freed and coworkers have provided biochemical evidence that MA trimerization is an obligatory step in the assembly of infectious HIV-1 and demonstrated a correlation between loss of MA trimerization and loss of Env incorporation (46). Nonconservative mutations at, or near, the trimer interface in the crystal structure (Fig. 1) inhibited MA trimerization and yielded particles with impaired Env incorporation and infectivity (46). Substitution of residue Gln^{63} with Arg suppressed Env incorporation defects of the L13E, E17K, L31E, V35E, and E99V MA mutations (44–46, 52). The current hypothesis suggests that Q63R mutation may stabilize the trimer structure such that MA lattices, which form large hexamer holes, are favored over those that feature small hexamer holes (Fig. 1) (46). This hypothesis was further supported by the finding that the Q63R mutation promoted interaction with gp41CT without altering the organization of MA on a membrane layer (43). A correlation between MA trimerization and gp41CT binding was also suggested in a biochemical study involving MA mutants and MACA proteins, supplemented with inositol polyphosphates (67).

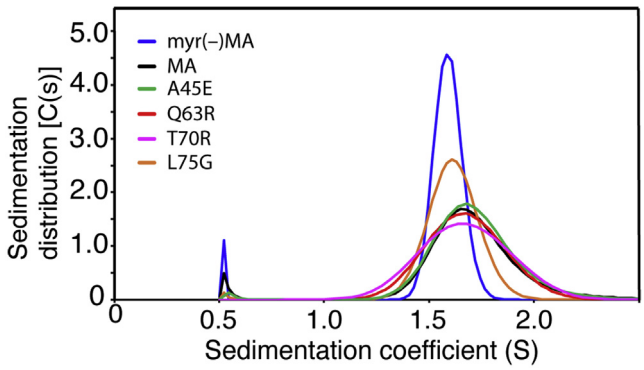

Figure 6. Sedimentation velocity data. Sedimentation coefficient distributions, c(s), obtained from the sedimentation profiles for WT and mutant MA proteins at pH 5.5.

Table 2
Monomer-trimer association constants for the WT and mutant MA proteins obtained from sedimentation equilibrium experiments at pH 5.5

MA protein	K_a ($\times 10^7$ M^{-1})
WT	2.0 ± 0.6
A45E	2.5 ± 0.3
Q63R	2.0 ± 0.2
T70R	2.8 ± 0.3
L75G	1.0 ± 0.1

Standard deviations were obtained from 2 or 3 replicates.

In this study, we have shown that: (i) mutations that either impaired (A45E, T70R, and L75G) or rescued (Q63R) Env incorporation had no adverse effects on the structures and folding of the MA protein. This result rules out the possibility that such mutations produce a nonfunctional protein that indirectly impacts its ability to form a trimer or participate in other functions involved in Env incorporation. (ii) None of the mutations had any detectable effect on the efficiency of myristoylation or concentration-dependent myr switch. NMR data obtained at different protein concentrations indicate that all four mutants display a concentration-dependent myr switch mechanism, similar to the WT MA protein. (iii) Mutations appear to induce minor structural perturbations in the trimer interface, which may directly or indirectly contribute to the (de)stabilization of the MA trimer form. As detected by NMR, the largest CSPs were observed for the L75G mutant. This result is not surprising given that Leu^{75} is located in an α-helical motif. Substitution with a glycine reside, which is sometimes known as a helix breaker, may have induced a larger structural change than the other three mutants. As mentioned earlier, the effect of Leu^{75} mutation on MA trimerization is probably indirect as this residue is not involved in intermolecular interactions with a neighboring MA molecule. Leu^{75} is in close proximity to Leu^{64}, which is in juxtaposition to the loop made of amino acid residues 67–72 that interacts with amino acid residues 42–46 of a neighboring molecule. Therefore, it is conceivable that Leu^{75} contributes to the orientation of this loop to enable interaction with an adjacent molecule. (iv) A new hydrogen bond is formed between the side chains of adjacent Arg^{63} and Ser^{67} residues on neighbouring MA molecules in the center of the trimer interface of myr(–)MA Q63R, providing the first structural evidence for an additional intermolecular interaction in the trimer interface. (v) SV and SE data show that the A45E, T70R, and Q63R mutations had minimal effect on the monomer–trimer equilibrium, whereas the L75G mutation enhanced the population of the monomeric form by twofold.

As discussed above, the structures of monomeric MA and myr(–)MA are nearly identical (21, 22, 25, 26, 68). The only distinct difference is that the X-ray structure of myr(–)MA revealed a trimer arrangement of MA molecules (21). The MA protein, however, is in monomer–trimer equilibrium. To determine whether the MA–MA interface in solution resembles that in the X-ray structure of myr(–)MA (21), we recently engineered a stable MA trimer by fusing a FD domain on the C-terminus of MA (28). Hydrogen–deuterium exchange MS data supported a MA–MA interface that is consistent with that observed in the crystal structure of the myr(–)MA trimer (28). Of note, the region that exhibited a significant increase in protection from deuteration in the HDX-MS assay is the same region identified here as a putative trimer interface. Our data presented here demonstrate that neither of the three mutants that were proposed to inhibit MA trimerization (A45E, T70R, and L75G) completely shifted the equilibrium to a monomer, nor did the Q63R mutation, which rescues Env incorporation, form a stable trimer in solution even though a new H-bond is observed between the side chains of Arg^{63} and Ser^{67} from neighboring subunits (Fig. 5). This discrepancy between the crystal structure and solution data is still not well understood. It is possible that other forces such as the position of the myr group and the conformation of the N-terminal helix may also influence the oligomerization properties. In the absence of detailed structural data of the myristoylated MA trimer, it is not possible to determine how all factors contribute to stabilization or destabilization of the trimer form. Furthermore, it is worth mentioning that the mutations that impair or rescue Env incorporations were studied in the context of full-length Gag. Other factors that were found to influence Gag oligomerization include the CA and SP1 domains, NC-RNA interaction, and membrane binding ([62, 69–71] and refs therein).

It is important to highlight the link between the structural findings and the previous biological findings. It is worth noting that previous studies indicated that residue Gln^{63} is not crucial for Env incorporation in the context of otherwise-WT MA and that Q63R is unique for its ability to fully rescue Env incorporation defects (44). It appears that the type of amino acid substitution at position Gln^{63} is key for its function in restoring Env incorporation. When introduced as a single mutation in MA, Q63R only minimally enhanced Env incorporation (44). However, the effect was more dramatic in restoring Env incorporation to a WT level when this mutation was introduced along with the Env-defective L13E mutant (44). By substituting Gln^{63} with E, G, K, L, N, or W, it was shown that all mutants replicated with WT kinetics in Jurkat cells and that none of the single mutations severely impaired virus release, infectivity, or Env incorporation. When the L13E/Q63[E/G/K/L/N/W] double mutants were subjected to the same analysis, none of the Gln^{63} mutants was able to fully rescue the virus replication, infectivity, and Env incorporation defects imposed by the L13E mutant (44). Interestingly, even the L13E/Q63K mutant exhibited a partial rescue, as infectivity in TZM-bl cells was comparable with that of L13E/Q63R, no rescue of Env incorporation was apparent. Taken together, Q63R appears to be unique for its ability to fully rescue Env incorporation defects. Our findings complemented the biological data by showing that the H-bond formed between the side chains of Arg^{63} and Ser^{67} is key for the stability of the MA trimer and hence to its function in rescuing Env incorporation (44). It is possible that slight changes to trimerization may be amplified in a biological context, due to the 2D constraint imposed by the membrane or the presence of other oligomerization promoting domains of Gag such as CA.

Role of Ser[67] and Thr[70] in Env incorporation in the context of WT, L13E, Q63R, and L13E/Q63R clones was also investigated (44). Whereas the S67A mutation had no effect on the phenotypes of the four viral clones, T70A blocked the ability of Q63R to rescue L13E infectivity and Env incorporation, although Q63R/T70A was as infectious as Q63R alone. The single T70A mutant was also impaired for infectivity and Env incorporation, suggesting that Thr[70] may be involved in MA function. Another interesting result is the finding that S67R behaved like Q63R in its ability to rescue the defect imposed by L13E, indicating that an Arg at either residue 63 or 67 could rescue the L13E defect (44). Based on the structure of the myr(−)MA Q63R protein (Fig. 5), it is clear that Ser[67] plays an important role in forming a H-bond with Arg[63]. It is expected that an Arg at position 67 is also capable of forming an H-bond with the side chain of Gln[63] on a neighboring molecule, therefore stabilizing the MA trimer structure. The close proximity of Arg[63] and Ser[67] and their role in the stabilization of the MA trimer are supported by the finding that MA forms dimer and trimer in the glutaraldehyde cross-linking assay conducted with the double mutant (Q63K/S67K) in Jurkat and MT4 cell lines (46).

Combining previous studies with the data presented here, it appears that the correlation between trimerization of the MA domain of Gag and Env incorporation is not straightforward. Mutation of residues located in the trimer interface, on the tip of the hexamer ring, or even distant residues can impact Env incorporation. In a recent study, new compensatory mutations that rescue MA trimer interface mutants with severely impaired Env incorporation in MT-4 T-cells were identified (47). Viruses with MA L75G mutation acquired mutations G11S, V35I/F44I, V35I/E52K, V46I, and E52K. For viruses with MA L75E mutation, compensatory mutations D14N/V45I, Q28K, V35I/F44L, and E52K were identified. Of note, among all these secondary mutations only Phe[44] and Val[46] are located in the trimer interface. It was suggested that mutations that are distant from the trimer interface may indirectly influence the trimer interface by inducing potential structural or conformational changes (47). Structural studies to discern conformational changes induced by the compensatory mutations are warranted.

Our data support the hypothesis that mutations in MA that block Env incorporation may do so by disrupting an otherwise-stable MA lattice, rather than by disrupting a specific MA–gp41 interaction. The importance of the trimer interface in rescuing Env incorporation suggests that a stable MA trimer is key to trap Env into the Gag lattice. This model is also supported by recent high-resolution single-molecule tracking data (72), which demonstrated that Env trimers are confined to subviral regions of a budding Gag lattice, supporting a model where direct interactions and steric corralling between the gp41CT and MA lattice promote Env trapping. In summary, the new findings advance our understanding of the complementary, yet distinct, roles the MA domain of Gag and gp41CT play in Env incorporation.

Experimental procedures

Plasmid construction and protein expression

A plasmid encoding for HIV-1 MA (pNL4-3 strain) and yeast N-terminal myristoyl transferase was provided by Dr Michael Summers (Howard Hughes Medical Institute, University of Maryland). The A45E, T70R, Q63R and L75G MA mutant constructs were generated using a QuickChange Lightning site-directed mutagenesis kit (Agilent Technologies). Forward and reverse primers (Integrated DNA Technologies) extended 15 base pairs on either side of the mutation codon. Mutations were verified by plasmid sequencing at the Heflin Genomics Core at the University of Alabama at Birmingham. WT and mutant MA and myr(−)MA proteins were prepared as described (22, 24–26).

NMR spectroscopy

NMR data were collected at 35 °C on a Bruker Avance II (700 MHz ^{1}H) or Avance III (600 or 850 MHz ^{1}H) spectrometers equipped with cryogenic triple-resonance probes, processed with NMRPIPE (73) and analyzed with NMRVIEW (74) or CCPN (75). The backbone resonances were assigned using standard triple resonance data (HNCA, HN(CO)CA, HN(CO)CACB, and HNCACB) collected at 35 °C on 100–300 μM samples in a buffer containing 50 mM sodium phosphates (pH 5.5), 50 mM NaCl, and 1 mM tris(2-carboxyethyl)phosphine hydrochloride (TCEP). The triple-resonance experiments were collected as nonuniformly sampled (NUS) sparse data (20% sampling density in indirect dimensions) according to schemes generated using hmsIST (76). Chemical shift perturbations were calculated as $\Delta\delta_{HN} = \sqrt{\Delta\delta_H^2 + 0.04\Delta\delta_N^2}$, where $\Delta\delta_H$ and $\Delta\delta_N$ are ^{1}H and ^{15}N chemical shift changes, respectively. Histograms for the chemical shift changes were generated using gnuplot software (http://www.gnuplot.info) (77). Structural representations of the chemical shift changes were generated using PyMOL (Schrödinger, LLC) (78).

X-ray crystallography and structure determination

The HIV-1 myr(−)MA Q63R protein used in the crystallization trials was at 20 mg/ml in a buffer containing 10 mM Tris.HCl (pH 8), 1 mM EDTA, 2 mM β-mercaptoethanol, and 50 mM NaCl. Diffraction quality crystals were obtained using hanging-drop vapor diffusion in a solution of 40% PEG (molecular weight 400), 0.1 M sodium acetate (pH 4), and 50 mM lithium sulfate. Crystals were cryo-cooled in the same conditions. X-ray diffraction data were collected at the Advance Photon Source, Southeast Regional Collaborative Access Team (SER-CAT) Beamline 22-ID. Raw intensity data were processed with the HKL2000 software package (79). The initial electron density map was generated *via* molecular replacement with PHASER (80) using the previously solved structure of the WT myr(−)MA protein (PDB code 1HIW). The structure was then iteratively refined with PHENIX (81) and Coot (82). Visualization of structures was performed using Pymol.

Analytical ultracentrifugation

Sedimentation velocity (SV) and sedimentation equilibrium (SE) experiments were performed on a Beckman XL-I Optima ultracentrifuge equipped with a four-hole An-60 rotor (Beckman Coulter). Cells were equipped with double-sector, charcoal-filled epon centerpieces with 12 mm path lengths and sapphire windows. Prior to AUC data collection, protein samples were run on a size-exclusion chromatography column (Superdex 75, 10/300GL, cytiva) in a buffer containing 50 mM sodium phosphates (pH 5.5), 100 mM NaCl, and 2 mM TCEP. Loading concentrations of MA samples ranged from 30 to 100 μM. For the SV experiments, rotor speed was set at 40,000 rpm. SE experiments were performed at 22,000, 26,000, and 30,000 rpm. All experiments were carried out at 20 °C. Scans were collected at a wavelength of 280 and 250 nm for the SV and SE experiments, respectively. Partial specific volumes (v-bar) and molar extinction coefficients were calculated by using the program SENDTERP, and buffer densities were measured pycnometrically. SV data were analyzed using SEDFIT (83–86), and SE data were analyzed with HETERO-ANALYSIS (87). Sedimentation coefficients obtained from SV experiments were corrected to 20 °C and infinite dilution in water ($s_{20,w}$). Equilibrium association constants were obtained by global fitting of SE scans collected at a single concentration and at three rotor speeds using a monomer–trimer equilibrium model. The molecular weight of the monomer (15.6 kDa) and the complex stoichiometry (n = 3) were treated as fixed parameters. Reference concentrations and baselines for each scan were floated parameters, and the K_a for the monomer–trimer equilibrium was fit as a global parameter.

Data availability

The atomic coordinates and structure factors (codes 7JXR and 7JXS) have been deposited in the Protein Data Bank (http://wwpdb.org/). The NMR chemical shift data for HIV-1 MA A45E, Q63R, L75G, and T70R are available from the Biological Magnetic Resonance Data Bank under BMRB accession numbers 50640, 50641, 50642, and 50643, respectively. The raw data described in the article can be shared upon request by directly contacting Saad@uab.edu.

Acknowledgments—We thank Dr Aaron Lucius (University of Alabama at Birmingham) for helping with the AUC experiments. We also thank the O'Neal Comprehensive Cancer Center at the University of Alabama at Birmingham (funded by grant P30 CA013148 from the National Institutes of Health, NIH) for supporting the High-Field NMR facility. X-ray data were collected at the SER-CAT 22-ID beamline at the Advanced Photon Source, Argonne National Laboratory. SER-CAT is supported by its member institutions and equipment grants (S10_RR25528 and S10_RR028976) from the NIH. Use of the Advanced Photon Source was supported by the U. S. Department of Energy, Office of Science, Office of Basic Energy Sciences, under Contract No. W-31-109-Eng-38.

Author contributions—G. N. E., R. H. G., T. J. G., and J. S. S. designed the experiments. G. N. E. and R. H. G. expressed, purified, and characterized the proteins. G. N. E. and J. S. S. performed the NMR experiments and analyzed the results. T. J. G. collected and analyzed the X-ray data. G. N. E. and J. S. S. wrote the paper. G. N. E., R. H. G., T. J. G., and J. S. S. edited the paper.

Funding and additional information—This work was supported by grants 5R01GM117837 and 9R01AI150901 from the NIH to J. S. S. The High-Field NMR facility at the University of Alabama at Birmingham was established through the NIH (1S10RR026478) and is currently supported by the O'Neal comprehensive cancer center (NIH grant P30 CA013148). The content is solely the responsibility of the authors and does not necessarily represent the official views of the NIH.

Conflict of interest—The authors declare that they have no conflicts of interest with the contents of this article.

Abbreviations—The abbreviations used are: AUC, analytical ultracentrifugation; CSP, chemical shift perturbation; HSQC, heteronuclear single quantum coherence; MA, myristoylated matrix; ER, endoplasmic reticulum; myr(−)MA, unmyristoylated matrix; NMR, nuclear magnetic resonance; PI(4,5)P_2, phosphatidylinositol 4,5-bisphosphate.

References:

1. Mücksch, F., Laketa, V., Muller, B., Schultz, C., and Krausslich, H. G. (2017) Synchronized HIV assembly by tunable PIP_2 changes reveals PIP_2 requirement for stable Gag anchoring. *Elife* **6**, e25287
2. Hendrix, J., Baumgartel, V., Schrimpf, W., Ivanchenko, S., Digman, M. A., Gratton, E., Krausslich, H. G., Muller, B., and Lamb, D. C. (2015) Live-cell observation of cytosolic HIV-1 assembly onset reveals RNA-interacting Gag oligomers. *J. Cell Biol.* **210**, 629–646
3. Gousset, K., Ablan, S. D., Coren, L. V., Ono, A., Soheilian, F., Nagashima, K., Ott, D. E., and Freed, E. O. (2008) Real-time visualization of HIV-1 GAG trafficking in infected macrophages. *PLoS Pathog.* **4**, e1000015
4. Jouvenet, N., Neil, S. J. D., Bess, C., Johnson, M. C., Virgen, C. A., Simon, S. M., and Bieniasz, P. D. (2006) Plasma membrane is the site of productive HIV-1 particle assembly. *PLoS Biol.* **4**, e435
5. Welsch, S., Keppler, O. T., Habermann, A., Allespach, I., Krijnse-Locker, J., and Kräusslich, H.-G. (2007) HIV-1 buds predominantly at the plasma membrane of primary human macrophages. *PLoS Pathog.* **3**, e36
6. Chukkapalli, V., Hogue, I. B., Boyko, V., Hu, W.-S., and Ono, A. (2008) Interaction between HIV-1 Gag matrix domain and phosphatidylinositol-(4,5)-bisphosphate is essential for efficient Gag-membrane binding. *J. Virol.* **82**, 2405–2417
7. Ono, A., Ablan, S. D., Lockett, S. J., Nagashima, K., and Freed, E. O. (2004) Phosphatidylinositol (4,5) bisphosphate regulates HIV-1 Gag targeting to the plasma membrane. *Proc. Natl. Acad. Sci. U. S. A.* **101**, 14889–14894
8. Chukkapalli, V., Inlora, J., Todd, G. C., and Ono, A. (2013) Evidence in support of RNA-mediated inhibition of phosphatidylserine-dependent HIV-1 Gag membrane binding in cells. *J. Virol.* **87**, 7155–7159
9. Chukkapalli, V., and Ono, A. (2011) Molecular determinants that regulate plasma membrane association of HIV-1 gag. *J. Mol. Biol.* **410**, 512–524
10. Purohit, P., Dupont, S., Stevenson, M., and Green, M. R. (2001) Sequence-specific interaction between HIV-1 matrix protein and viral genomic RNA revealed by *in vitro* genetic selection. *RNA* **7**, 576–584
11. Li, H., Dou, J., Ding, L., and Spearman, P. (2007) Myristoylation is required for human immunodeficiency virus type 1 Gag-Gag multimerization in mammalian cells. *J. Virol.* **81**, 12899–12910
12. Dalton, A. K., Ako-Adjei, D., Murray, P. S., Murray, D., and Vogt, M. V. (2007) Electrostatic interactions drive membrane association of the human immunodeficiency virus type 1 gag MA domain. *J. Virol.* **81**, 6434–6445

13. Dick, R. A., Goh, S. L., Feigenson, G. W., and Vogt, V. M. (2012) HIV-1 Gag protein can sense the cholesterol and acyl chain environment in model membranes. *Proc. Natl. Acad. Sci. U. S. A.* **109**, 18761–18767
14. Waheed, A. A., and Freed, E. O. (2009) Lipids and membrane microdomains in HIV-1 replication. *Virus Res.* **143**, 162–176
15. Chukkapalli, V., Oh, S. J., and Ono, A. (2010) Opposing mechanisms involving RNA and lipids regulate HIV-1 Gag membrane binding through the highly basic region of the matrix domain. *Proc. Natl. Acad. Sci. U. S. A.* **107**, 1600–1605
16. Waheed, A. A., and Freed, E. O. (2010) The role of lipids in retrovirus replication. *Viruses* **2**, 1146–1180
17. Ono, A. (2010) HIV-1 assembly at the plasma membrane. *Vaccine* **28 Suppl 2**, B55–B59
18. Chan, J., Dick, R. A., and Vogt, V. M. (2011) Rous sarcoma virus gag has No specific requirement for phosphatidylinositol-(4,5)-bisphosphate for plasma membrane association in vivo or for liposome interaction in vitro. *J. Virol.* **85**, 10851–10860
19. Alfadhli, A., Still, A., and Barklis, E. (2009) Analysis of human immunodeficiency virus type 1 matrix binding to membranes and nucleic acids. *J. Virol.* **83**, 12196–12203
20. Barros, M., Heinrich, F., Datta, S. A., Rein, A., Karageorgos, I., Nanda, H., and Losche, M. (2016) Membrane binding of HIV-1 matrix protein: Dependence on bilayer composition and protein lipidation. *J. Virol.* **90**, 4544–4555
21. Hill, C. P., Worthylake, D., Bancroft, D. P., Christensen, A. M., and Sundquist, W. I. (1996) Crystal structures of the trimeric HIV-1 matrix protein: Implications for membrane association. *Proc. Natl. Acad. Sci. U. S. A.* **93**, 3099–3104
22. Massiah, M. A., Starich, M. R., Paschall, C., Summers, M. F., Christensen, A. M., and Sundquist, W. I. (1994) Three dimensional structure of the human immunodeficiency virus type 1 matrix protein. *J. Mol. Biol.* **244**, 198–223
23. Mercredi, P. Y., Bucca, N., Loeliger, B., Gaines, C. R., Mehta, M., Bhargava, P., Tedbury, P. R., Charlier, L., Floquet, N., Muriaux, D., Favard, C., Sanders, C. R., Freed, E. O., Marchant, J., and Summers, M. F. (2016) Structural and molecular determinants of membrane binding by the HIV-1 matrix protein. *J. Mol. Biol.* **428**, 1637–1655
24. Saad, J. S., Loeliger, E., Luncsford, P., Liriano, M., Tai, J., Kim, A., Miller, J., Joshi, A., Freed, E. O., and Summers, M. F. (2007) Point mutations in the HIV-1 matrix protein turn off the myristyl switch. *J. Mol. Biol.* **366**, 574–585
25. Saad, J. S., Miller, J., Tai, J., Kim, A., Ghanam, R. H., and Summers, M. F. (2006) Structural basis for targeting HIV-1 Gag proteins to the plasma membrane for virus assembly. *Proc. Natl. Acad. Sci. U. S. A.* **103**, 11364–11369
26. Tang, C., Loeliger, E., Luncsford, P., Kinde, I., Beckett, D., and Summers, M. F. (2004) Entropic switch regulates myristate exposure in the HIV-1 matrix protein. *Proc. Natl. Acad. Sci. U. S. A.* **101**, 517–522
27. Fledderman, E. L., Fujii, K., Ghanam, R. H., Waki, K., Prevelige, P. E., Freed, E. O., and Saad, J. S. (2010) Myristate exposure in the human immunodeficiency virus type 1 matrix protein is modulated by pH. *Biochemistry* **49**, 9551–9562
28. Murphy, R. E., Samal, A. B., Vlach, J., Mas, V., Prevelige, P. E., and Saad, J. S. (2019) Structural and biophysical characterizations of HIV-1 matrix trimer binding to lipid nanodiscs shed light on virus assembly. *J. Biol. Chem.* **294**, 18600–18612
29. Guthe, S., Kapinos, L., Moglich, A., Meier, S., Grzesiek, S., and Kiefhaber, T. (2004) Very fast folding and association of a trimerization domain from bacteriophage T4 fibritin. *J. Mol. Biol.* **337**, 905–915
30. Meier, S., Guthe, S., Kiefhaber, T., and Grzesiek, S. (2004) Foldon, the natural trimerization domain of T4 fibritin, dissociates into a monomeric A-state form containing a stable beta-hairpin: Atomic details of trimer dissociation and local beta-hairpin stability from residual dipolar couplings. *J. Mol. Biol.* **344**, 1051–1069
31. Vlach, J., and Saad, J. S. (2013) Trio engagement via plasma membrane phospholipids and the myristoyl moiety governs HIV-1 matrix binding to bilayers. *Proc. Natl. Acad. Sci. U. S. A.* **110**, 3525–3530
32. Saad, J. S., Ablan, S. D., Ghanam, R. H., Kim, A., Andrews, K., Nagashima, K., Soheilian, F., Freed, E. O., and Summers, M. F. (2008) Structure of the myristylated HIV-2 MA protein and the role of phosphatidylinositol-(4,5)-bisphosphate in membrane targeting. *J. Mol. Biol.* **382**, 434–447
33. Vlach, J., Eastep, G. N., Ghanam, R. H., Watanabe, S. M., Carter, C. A., and Saad, J. S. (2018) Structural basis for targeting avian sarcoma virus Gag polyprotein to the plasma membrane for virus assembly. *J. Biol. Chem.* **293**, 18828–18840
34. Hamard-Peron, E., Juillard, F., Saad, J. S., Roy, C., Roingeard, P., Summers, M. F., Darlix, J. L., Picart, C., and Muriaux, D. (2010) Targeting of murine leukemia virus gag to the plasma membrane is mediated by PI(4,5)P_2/PS and a polybasic region in the matrix. *J. Virol.* **84**, 503–515
35. Stansell, E., Apkarian, R., Haubova, S., Diehl, W. E., Tytler, E. M., and Hunter, E. (2007) Basic residues in the Mason-Pfizer monkey virus gag matrix domain regulate intracellular trafficking and capsid-membrane interactions. *J. Virol.* **81**, 8977–8988
36. Prchal, J., Srb, P., Hunter, E., Ruml, T., and Hrabal, R. (2012) The structure of myristoylated Mason-Pfizer monkey virus matrix protein and the role of phosphatidylinositol-(4,5)-bisphosphate in its membrane binding. *J. Mol. Biol.* **423**, 427–438
37. Brown, L. A., Cox, C., Baptiste, J., Summers, H., Button, R., Bahlow, K., Spurrier, V., Kyser, J., Luttge, B. G., Kuo, L., Freed, E. O., and Summers, M. F. (2015) NMR structure of the myristylated feline immunodeficiency virus matrix protein. *Viruses* **7**, 2210–2229
38. Anraku, K., Fukuda, R., Takamune, N., Misumi, S., Okamoto, Y., Otsuka, M., and Fujita, M. (2010) Highly sensitive analysis of the interaction between HIV-1 Gag and phosphoinositide derivatives based on surface plasmon resonance. *Biochemistry* **49**, 5109–5116
39. Shkriabai, N., Datta, S. A., Zhao, Z., Hess, S., Rein, A., and Kvaratskhelia, M. (2006) Interactions of HIV-1 Gag with assembly cofactors. *Biochemistry* **45**, 4077–4083
40. Fernandes, F., Chen, K., Ehrlich, L. S., Jin, J., Chen, M. H., Medina, G. N., Symons, M., Montelaro, R., Donaldson, J., Tjandra, N., and Carter, C. A. (2011) Phosphoinositides direct equine infectious anemia virus gag trafficking and release. *Traffic* **12**, 438–451
41. Alfadhli, A., Barklis, R. L., and Barklis, E. (2009) HIV-1 matrix organizes as a hexamer of trimers on membranes containing phosphatidylinositol-(4,5)-bisphosphate. *Virology* **387**, 466–472
42. Alfadhli, A., Huseby, D., Kapit, E., Colman, D., and Barklis, E. (2007) Human immunodeficiency virus type 1 matrix protein assembles on membranes as a hexamer. *J. Virol.* **81**, 1472–1478
43. Alfadhli, A., Mack, A., Ritchie, C., Cylinder, I., Harper, L., Tedbury, P. R., Freed, E. O., and Barklis, E. (2016) Trimer enhancement mutation effects on HIV-1 matrix protein binding activities. *J. Virol.* **90**, 5657–5664
44. Tedbury, P. R., Ablan, S. D., and Freed, E. O. (2013) Global rescue of defects in HIV-1 envelope glycoprotein incorporation: Implications for matrix structure. *PLoS Pathog.* **9**, e1003739
45. Tedbury, P. R., and Freed, E. O. (2014) The role of matrix in HIV-1 envelope glycoprotein incorporation. *Trends Microbiol.* **22**, 372–378
46. Tedbury, P. R., Novikova, M., Ablan, S. D., and Freed, E. O. (2016) Biochemical evidence of a role for matrix trimerization in HIV-1 envelope glycoprotein incorporation. *Proc. Natl. Acad. Sci. U. S. A.* **113**, E182–E190
47. Tedbury, P. R., Novikova, M., Alfadhli, A., Hikichi, Y., Kagiampakis, I., KewalRamani, V. N., Barklis, E., and Freed, E. O. (2019) HIV-1 matrix trimerization-impaired mutants are rescued by matrix substitutions that enhance envelope glycoprotein incorporation. *J. Virol.* **94**, e01526-01519
48. Checkley, M. A., Luttge, B. G., and Freed, E. O. (2011) HIV-1 envelope glycoprotein biosynthesis, trafficking, and incorporation. *J. Mol. Biol.* **410**, 582–608
49. Chen, B. (2019) Molecular mechanism of HIV-1 entry. *Trends Microbiol.* **27**, 878–891
50. Wang, Q., Finzi, A., and Sodroski, J. (2020) The conformational states of the HIV-1 envelope glycoproteins. *Trends Microbiol.* **28**, 655–667
51. Tedbury, P. R., and Freed, E. O. (2015) The cytoplasmic tail of retroviral envelope glycoproteins. *Prog. Mol. Biol. Transl Sci.* **129**, 253–284
52. Tedbury, P. R., Mercredi, P. Y., Gaines, C. R., Summers, M. F., and Freed, E. O. (2015) Elucidating the mechanism by which compensatory mutations

rescue an HIV-1 matrix mutant defective for gag membrane targeting and envelope glycoprotein incorporation. *J. Mol. Biol.* **427**, 1413–1427
53. Akari, H., Fukumori, T., and Adachi, A. (2000) Cell-dependent requirement of human immunodeficiency virus type 1 gp41 cytoplasmic tail for Env incorporation into virions. *J. Virol.* **74**, 4891–4893
54. Murakami, T., and Freed, E. O. (2000) The long cytoplasmic tail of gp41 is required in a cell type-dependent manner for HIV-1 envelope glycoprotein incorporation into virions. *Proc. Natl. Acad. Sci. U. S. A.* **97**, 343–348
55. Murphy, R. E., Samal, A. B., Vlach, J., and Saad, J. S. (2017) Solution structure and membrane interaction of the cytoplasmic tail of HIV-1 gp41 protein. *Structure* **25**, 1708–1718.e1705
56. Piai, A., Fu, Q., Cai, Y., Ghantous, F., Xiao, T., Shaik, M. M., Peng, H., Rits-Volloch, S., Chen, W., Seaman, M. S., Chen, B., and Chou, J. J. (2020) Structural basis of transmembrane coupling of the HIV-1 envelope glycoprotein. *Nat. Commun.* **11**, 2317
57. Dorfman, T., Mammano, F., Haseltine, W. A., and Göttlinger, H. G. (1994) Role of the matrix protein in the virion association of the human immunodeficiency virus type 1 envelope glycoprotein. *J. Virol.* **68**, 1689–1696
58. Freed, E. O., and Martin, A. M. (1996) Domains of the human immonodeficiency virus type 1 matrix and gp41 cytoplasmic tail required for envelope incorporation into virions. *J. Virol.* **70**, 341–351
59. Freed, O. E., and Martin, A. M. (1995) Virion incorporation of envelope glycoproteins with long but not short cytoplasmic tails is blocked by specific, single amino acid substitutions in the human immunodeficiency virus type 1 matrix. *J. Virol.* **69**, 1984–1989
60. Yu, X., Yuan, X., Matsuda, Z., Lee, T.-H., and Essex, M. (1992) The matrix protein of human immunodeficiency virus type I is required for incorporation of viral envelope protein into mature virions. *J. Virol.* **66**, 4966–4971
61. Cosson, P. (1996) Direct interaction between the envelope and matrix proteins of HIV-1. *EMBO J.* **15**, 5783–5788
62. Murphy, R. E., and Saad, J. S. (2020) The interplay between HIV-1 gag binding to the plasma membrane and Env incorporation. *Viruses* **12**, 548
63. Freed, E. O., Orenstein, J. M., Buckler-White, A. J., and Martin, M. A. (1994) Single amino acid changes in the human immunodeficiency virus type 1 matrix protein block virus particle production. *J. Virol.* **68**, 5311–5320
64. Ono, A., and Freed, E. O. (1999) Binding of human immunodeficiency virus type 1 gag to membrane: Role of the matrix amino terminus. *J. Virol.* **73**, 4136–4144
65. Ono, A., Huang, M., and Freed, E. O. (1997) Characterization of human immunodeficiency virus type 1 matrix revertants: Effects on virus assembly, Gag processing, and Env incorporation into virions. *J. Virol.* **71**, 4409–4418
66. Paillart, J.-C., and Gottlinger, H. G. (1999) Opposing effects of human immunodeficiency virus type 1 matrix mutations support a myristyl switch model of Gag membrane targeting. *J. Virol.* **73**, 2604–2612
67. Alfadhli, A., Staubus, A. O., Tedbury, P. R., Novikova, M., Freed, E. O., and Barklis, E. (2019) Analysis of HIV-1 matrix-envelope cytoplasmic tail interactions. *J. Virol.* **93**, e01079-01019
68. Massiah, M. A., Worthylake, D., Christensen, A. M., Sundquist, W. I., Hill, C. P., and Summers, M. F. (1996) Comparison of the NMR and X-ray structures of the HIV-1 matrix protein: Evidence for conformational changes during viral assembly. *Protein Sci.* **5**, 2391–2398
69. Dick, R. A., Zadrozny, K. K., Xu, C., Schur, F. K. M., Lyddon, T. D., Ricana, C. L., Wagner, J. M., Perilla, J. R., Ganser-Pornillos, B. K., Johnson, M. C., Pornillos, O., and Vogt, V. M. (2018) Inositol phosphates are assembly co-factors for HIV-1. *Nature* **560**, 509–512
70. Ganser-Pornillos, B. K., Yeager, M., and Pornillos, O. (2012) Assembly and architecture of HIV. *Adv. Exp. Med. Biol.* **726**, 441–465
71. Pak, A. J., Grime, J. M. A., Sengupta, P., Chen, A. K., Durumeric, A. E. P., Srivastava, A., Yeager, M., Briggs, J. A. G., Lippincott-Schwartz, J., and Voth, G. A. (2017) Immature HIV-1 lattice assembly dynamics are regulated by scaffolding from nucleic acid and the plasma membrane. *Proc. Natl. Acad. Sci. U. S. A.* **114**, E10056–E10065
72. Pezeshkian, N., Groves, N. S., and van Engelenburg, S. B. (2019) Single-molecule imaging of HIV-1 envelope glycoprotein dynamics and Gag lattice association exposes determinants responsible for virus incorporation. *Proc. Natl. Acad. Sci. U. S. A.* **116**, 25269–25277
73. Delaglio, F., Grzesiek, S., Vuister, G. W., Zhu, G., Pfeifer, J., and Bax, A. (1995) NMRPipe: A multidimensional spectral processing system based on UNIX pipes. *J. Biomol. NMR* **6**, 277–293
74. Johnson, B. A., and Blevins, R. A. (1994) NMRview: A computer program for the visualization and analysis of NMR data. *J. Biomol. NMR* **4**, 603–614
75. Vranken, W. F., Boucher, W., Stevens, T. J., Fogh, R. H., Pajon, A., Llinas, M., Ulrich, E. L., Markley, J. L., Ionides, J., and Laue, E. D. (2005) The CCPN data model for NMR spectroscopy: Development of a software pipeline. *Proteins* **59**, 687–696
76. Hyberts, S. G., Milbradt, A. G., Wagner, A. B., Arthanari, H., and Wagner, G. (2012) Application of iterative soft thresholding for fast reconstruction of NMR data non-uniformly sampled with multidimensional Poisson Gap scheduling. *J. Biomol. NMR* **52**, 315–327
77. Racine, J. (2006) Gnuplot 4.0: A portable interactive plotting utility. *J. Appl. Econom.* **21**, 133–141
78. DeLano, W. L. (2002) *The PyMOL Molecular Graphics System*, DeLano Scientific, San Carlos, CA
79. Otwinowski, Z., and Minor, W. (1997) Processing of X-ray diffraction data collected in oscillation mode. *Methods Enzymol.* **276**, 307–326
80. McCoy, A. J., Grosse-Kunstleve, R. W., Adams, P. D., Winn, M. D., Storoni, L. C., and Read, R. J. (2007) Phaser crystallographic software. *J. Appl. Crystallogr.* **40**, 658–674
81. Adams, P. D., Afonine, P. V., Bunkoczi, G., Chen, V. B., Davis, I. W., Echols, N., Headd, J. J., Hung, L. W., Kapral, G. J., Grosse-Kunstleve, R. W., McCoy, A. J., Moriarty, N. W., Oeffner, R., Read, R. J., Richardson, D. C., *et al*. (2010) PHENIX: A comprehensive Python-based system for macromolecular structure solution. *Acta Crystallogr. D Biol. Crystallogr.* **66**, 213–221
82. Emsley, P., Lohkamp, B., Scott, W. G., and Cowtan, K. (2010) Features and development of Coot. *Acta Crystallogr. D Biol. Crystallogr.* **66**, 486–501
83. Lebowitz, J., Lewis, M. S., and Schuck, P. (2002) Modern analytical ultracentrifugation in protein science - a tutorial review. *Protein Sci.* **11**, 2067–2079
84. Schuck, P. (2000) Size distribution analysis of macromolecules by sedimentation velocity ultracentrifugation and Lamm equation modeling. *Biophys. J.* **78**, 1606–1619
85. Schuck, P. (2003) On the analysis of protein self-association by sedimentation velocity analytical ultracentrifugation. *Anal. Biochem.* **320**, 104–124
86. Schuck, P., Perugini, M. S., Gonzales, N. R., Howlett, G. J., and Schubert, D. (2002) Size-distribution analysis of proteins by analytical ultracentrifugation: Strategies and application to model systems. *Biophys. J.* **82**, 1096–1111
87. Cole, J. L. (2004) Analysis of heterogeneous interactions. *Methods Enzymol.* **384**, 212–232